ESA Contract Report

ESA contract no 4000145264/24/NL/IB/ab

Contract Report to the European Space Agency

Evaluation of hyperspectral microwave observations for global NWP: Representation of expected uncertainties

Authors: Katie Lean, Niels Bormann and Sanjee Panditharatne

Mar 2026 (Final version)

Series: ECMWF ESA Contract Report Series

A full list of ECMWF Publications can be found on our web site under:
http://www.ecmwf.int/en/publications/

Contact: library@ecmwf.int

Contents

Abstract

In preparation for assessing the impact of a future hyperspectral microwave (hyperMW) sounding instrument on global Numerical Weather Prediction (NWP), it is essential to adequately define the expected instrument uncertainties. Accurate uncertainty estimates are particularly important for obtaining realistic results from the Ensemble of Data Assimilations (EDA) framework, which will be used for the impact evaluation. Two key aspects are addressed here: the application of initial perturbations to simulated brightness temperatures (BTs) and the specification of an accompanying observation error model. Simulated BTs are perturbed using random and correlated components of instrument noise, based on pre-launch estimates for the Hyperspectral Microwave Sounder (HyMS). Noise-equivalent delta temperature (NEDT) values of 0.53 K and 0.54 K are used for the temperature- and humidity-sounding bands respectively, following super-obbing of nine fields of view. As the correlations reduce rapidly with channel separation, only nearest and next nearest neighbour noise correlations are used. Background departures reveal noisier behaviour than for current broadband sensors, as expected, particularly in temperature-sounding channels. The hyperMW observations are assimilated within an all-sky framework where the accompanying error model accounts for increased observation error in the presence of cloud. Cloud signals are estimated using indicators derived from single low-noise broadband super-channels centred at 52.80 and 190.32 GHz for the temperature and humidity bands, respectively. These indicators capture larger representation errors well, as demonstrated by their relationship with the standard deviation of background departures. However, for higher-peaking temperature-sounding channels, cloud-related representation errors are small relative to instrument noise, making constant errors more appropriate than the situation-dependent errors used for heritage sensors. Strong inter-channel error correlations are present, particularly in the humidity band, with many off-diagonal values exceeding 0.5 in clear-sky and 0.9 in cloudy conditions. Recent technical advances at ECMWF now allow such correlations to be explicitly included in the all-sky assimilation scheme. Further EDA sensitivity experiments will refine the error settings and determine the final assimilation configuration.

1 Introduction

The introduction of hyperspectral technology for microwave (MW) sounders enables an instrument design that differs substantially from the current, long-established MW sounding instruments. Compared to the current heritage MW sensors, a new hyperspectral MW (hyperMW) instrument could provide a much denser distribution of vertical sensitivity. The fine spectral resolution allows the possibility to probe fine features in the absorption spectrum, particularly in the 50 GHz oxygen band, in addition to covering parts of the spectrum not currently sampled. One-dimension variational content studies have shown encouraging results for the potential forecast impact benefits of a hyperMW instrument (a review of the results is discussed in Lean and Bormann (2025)). In this project, we aim to evaluate, for the first time, the impact of a hyperMW instrument in a global NWP context. The outcomes are intended to assist in refining requirements and provide guidance in shaping the components of a future MW constellation.

The benefit of a new hyperMW instrument to global NWP will be assessed by the Ensemble of Data Assimilations (EDA) method. This builds on experience applying the technique to investigate potential future MW sounding instruments (Lean et al., 2026b; Ma et al., 2025; Lean et al., 2025). The EDA is a Monte Carlo approach which is used to estimate reductions in analysis or forecast uncertainties and can be applied to changes in both simulated and real observations (Lean et al., 2025; Harnisch et al., 2013; Tan et al., 2007). The EDA consists of an ensemble of 4D-Var assimilation systems where the initial conditions (observations, forecast model and sea surface temperature) are perturbed to generate the different ensemble members. The benefit (or degradation) from a change to the observing system is measured by the reduction in EDA spread – the variation of the members about the ensemble mean. In this study, observations from a potential future hyperMW instrument will be simulated and assimilated

with EDA experiments. EDA spread from changes to the real MW sounders will be used to provide context to impacts from the hyperMW instrument. The hypothetical instrument evaluated in this study is based on the Hyperspectral Microwave Sounder (HyMS) instrument developed by Spire Global Inc. (Spire) and Rutherford Appleton Laboratory Space (RAL Space) (Henry et al., 2023). HyMS has been launched in early 2026, becoming the first space-borne hyperMW instrument. This is intended as a demonstrator mission, providing the first experience of this novel technology on a satellite.

Gaining realistic impacts as indicated by the EDA spread changes is reliant on two important aspects:

1. The simulated observations should follow an appropriate simulation/assimilation strategy.
2. Suitable representation of the expected uncertainties i.e. realistic simulated brightness temperatures (BTs) and adequate estimates of the associated observation errors.

To address the first point, the strategy to simulate/assimilate the hyperMW data will use the current MW assimilation scheme as guidance. However, new challenges for assimilation are encountered with the hyperspectral technology that require careful consideration. These include quality control choices for quasi-continuous frequency sampling and issues related to radiative transfer modelling (further discussed in Lean and Bormann (2025)). Regarding the second point, the assigned observations errors are used in the generation of perturbations to the observations as part of the initial conditions for the EDA. In this way, the observation errors can influence the spread of the ensemble members within the assimilation window. Accordingly, the EDA spread characteristics at analysis/forecast lead times are sensitive to these perturbations. The observation errors also affect the weighting of the observations as they are assimilated in the 4D-Var system of each ensemble member. The all-sky observation error model (Geer and Bauer, 2011; Geer et al., 2014) will be adapted for the hyperMW instrument, where observation errors increase in the presence of cloudy signals.

Experience with current MW and hyperspectral infrared (IR) instruments has highlighted the presence of horizontal and vertical error correlations, the latter more commonly known as inter-channel error correlations due to the sensitivity of different channels to different atmospheric layers (e.g. Weston et al. (2014); Janjic et al. (2018)). Accounting for them explicitly or indirectly e.g. through error inflation can be beneficial (Ishibashi, 2024; Geer, 2019; Weston and Bormann, 2018). Inter-channel error correlations can be especially significant for humidity or cloud-sensitive channels due to larger representation errors arising, for instance, from scale mismatches or forward modelling errors, particularly in cloudy regions. Developing the technical capability for assimilating MW sounding instruments in the all-sky framework with explicitly defined inter-channel correlations has been the focus of recent work at ECMWF (Steele et al., 2025). Early testing with the Advanced Technology Microwave Sounder (ATMS) instrument has shown limited benefit, mostly confined to the Southern Hemisphere, for using the new scheme. However, for HyMS, which has a far larger number of cloud sensitive channels, inter-channel correlations could form a more significant contribution to the observation error. Therefore, we will consider strategies for accounting for such correlations either implicitly through error inflation or the feasibility of extending the recently available framework for an explicit definition.

In this report, we will present the work on defining the expected uncertainties for a hyperMW sensor. The final assimilation settings with be presented in a subsequent report to accompany the EDA evaluation and conclusions. A brief summary of the HyMS instrument, BT simulation and technical details for the experimental set up are given in section 2. The generation of the initial perturbations to the simulated BTs will be presented in section 3. The all-sky observation error model is introduced and adaptations for estimating the cloudy signals using frequencies on the hyperMW instrument described in section 4. The method for deriving the all-sky error model parameters is also presented. Consideration of the

inter-channel error correlations is discussed in section 5 and a summary and next steps in the project are presented in section 6.

2 Test configuration for simulation/assimilation

2.1 HyMS instrument details

The HyMS instrument (Henry et al., 2023) will provide the basis for the hyperMW sounding instrument in this study. An overview of the instrument with focus on details pertinent to this study can be found in Lean and Bormann (2025). Further details on the instrument design including comparison to an ATMS sensor have been replicated here for reference in table 1. In addition to the high-resolution channels on HyMS, three additional "super channels" have been created for this study which mimic lower noise, broadband channels on the heritage sensors (more details discussed later in section 3.1). These have central frequencies at 50.30, 52.80 and 190.32 GHz which resemble Advanced Microwave Sounding Unit-A (AMSU-A) channels 3 and 4 and Microwave Humidity Sounder (MHS) channel 5 respectively. Neighbouring channels with similar vertical sensitivity are averaged together with the number of channels chosen to reproduce as closely as possible the corresponding bandwidths on the heritage sensors. These channels will be important to characterise cloud contributions for the observation error model discussed in section 4.2 and for the retrieval of surface emissivity over land (using 50.3 GHz). Note that these super channels will only be used passively for auxiliary information and not intended for active assimilation.

2.2 Simulation and experiment configurations

For this study, we adapt the framework developed for simulation of MW sensors in earlier work (Lean et al., 2026b, 2025) to process a hyperMW instrument. Observations are simulated from high-resolution ($T_{Co}1279$, ∼9km, 137 vertical levels) ECMWF analysis trajectories using RTTOV[1] (version 14.0) (Saunders et al., 2018, 2020; Hocking et al., 2025) which contains MW scattering capabilities for all-sky treatment i.e. use in cloudy and clear situations. The Fast Microwave Ocean Surface Emissivity Mode - 6 (FASTEM-6) (Kazumori and English, 2015) and emissivity atlases (Karbou et al., 2006) (for simulation purposes) are used for surface emissivity modelling over ocean and land respectively. Spatial and temporal sampling reflects the HyMS orbits (table 1). All channels are assumed to have the same geolocation.

For the assimilation of the hyperMW data, the first 845 channels of the temperature-sounding band (up to 53.61 GHz) are screened out to avoid observations with strong surface-sensitivity, and all remaining channels will be used at the high spectral resolution offered by HyMS. By using as many channels as possible at the high spectral resolution, we aim to maximise the potential information content. However, we also follow the more conservative, and well-established geographical screening of the current MW sounders. The sophistication of the current assimilation system can be a limitation in general for assessing future satellites. The lower frequencies on HyMS have potential to improve the lower troposphere/planetary boundary layer (Gambacorta et al., 2023; Maddy et al., 2024) and future advances e.g. with more surface sensitive frequencies could enable additional impact in global NWP in the future.

The new super channels (see also table 2) are simulated by specifying three new channels to the RTTOV coefficient files. Parameters defined for these channels, allowing the conversion between observations

[1]RTTOV = Radiative Transfer for TOVS, TOVS = TIROS Operational Vertical Sounder, TIROS = Television Infrared Observation Satellite

Table 1: Summary of key information for the HyMS instrument (kindly provided courtesy of Spire). *Channels in the 183 GHz band have already been combined into bins of 8 neighbouring channels.

Instrument characteristic	HyMS	ATMS
Number of channels	1689 channels 49.42-57.75 GHz, 1 x 89 GHz and 212* x 183.13-191.55 GHz	13 channels 50.3 – 57.62 GHz, 5 channels 182.31–190.31 GHz, 1 x 23.8, 31.4, 88.2, 165.5 GHz
Channel bandwidths	6.34 MHz for 50-60 GHz, 40 MHz for 183 GHz	155-400 MHz for tropospheric 50 GHz, 500-2000 MHz for 183 GHz
Polarisation	50 GHz: vertical, 183 GHz: Horizontal	Horizontal for all 50 and 183 GHz channels
Number of pixels per scan line	45	96
Maximum scan angle	45 deg	52.7 deg
Scan duration	2.55 s	8/3 s
Local equator crossing time	1700	1330
Orbit height	500 km	824 km
Footprint size	33 km at 50 GHz band, 18 km at 183 GHz	32 km at 50 GHz 16 km at 183 GHz

and model BT equivalents, are based on combining the spectral response functions of the individual channels being grouped. The simulation/assimilation system therefore effectively treats these as if they were actual instrument channels, generating model BT equivalents directly rather than explicitly averaging the BTs of the relevant channels. Averaging the simulated BTs from the high-resolution channels would be more accurate however, we take the pragmatic decision to combine channels through the spectral response functions. Adding the option to handle averaged BTs and the model equivalents within the assimilation system is not straightforward. Differences in the eventual simulated BTs from the two approaches are expected to be very small.

In the simulation process, all available channels from HyMS are produced i.e. a total of 1905 channels. To handle the potentially huge data volume, spatial/temporal thinning usually applied after simulation in previous future MW satellite studies, is instead performed here prior to simulation. Following the choices for conventional MW sensors, HyMS observations are sub-sampled to simulate super-obbing (further details in section 3.1) and subject to thinning in space/time. The thinning step selects only the observation closest to a T_L255 (80 km) reduced Gaussian grid within a 30-minute time slot.

When generating the background departures presented in this report (i.e. comparison between observations (simulated or real) and a short-range 12h forecast referred to as the model background) the standard ECMWF research configuration of a deterministic 4D-Var assimilation experiment is used. This employs a $T_{Co}399$ (28km) resolution grid with 137 vertical levels and three inner loops at a resolution of $T_L95/T_L159/T_L255$ (210/125/80 km). The simulated hyperMW data are used in the all-sky framework. As for the simulation, FASTEM-6 is used for surface emissivity modelling over ocean. Over land/snow/sea-ice, a dynamic surface emissivity retrieval (Karbou et al., 2006) is performed where for

Table 2: Summary of key information for the HyMS frequency bands (kindly provided courtesy of Spire). The sample NEDT values are given which correspond to scaled values of the 3 dB Field of View (FOV) NEDT, accounting for the sampling interval of the instrument (Atkinson, 2015). Values are also given for the effective noise reduction after mimicking 3x3 averaging (see main text for more details). *Channels in the 183 GHz band have already been combined into bins of 8 neighbouring channels. **Broadband channels include 3 super channels created by averaging groups of high-resolution channels.

Characteristics	Temp-sounding band	Broadband channels	Humidity-sounding band
Number of channels	1689	4**	212*
Frequency range	49.42-57.75 GHz	50.30/52.80/89/190.32 GHz	183.13-191.55 GHz
Bandwidth	6.34 MHz	180.56/400.16/3000/2000 MHz	40 MHz
NEDT	1.60 K	0.26/0.18/0.15/0.23 K	1.63 K
NEDT after "3x3 averaging"	0.53 K	0.08/0.06/0.05/0.08 K	0.54 K

temperature-sounding channel, the retrieval is performed using the low-noise super channel centred at 50.3 GHz. For humidity-sounding channels, a broadband channel at 89 GHz is used over snow-free land similar to current sensors. Emissivity for humidity-sounding channels over snow/sea-ice surfaces is usually retrieved from 150 GHz however this is unavailable on HyMS, which forms the basis for the instrument in this study. As finding an alternative method of emissivity estimation over these difficult surfaces is challenging, a pragmatic approach is employed that will screen any channels with significant surface sensitivity in these regions. This could be revisited with real satellite observations in the future.

The final assimilation settings (e.g. channel selection for quality control) for the hyperMW instrument are still in refinement and preliminary experiment settings have been applied that are sufficient for the analysis presented here. For investigation and tuning e.g. of observation error models, the background departures tend to be subject to broad quality control measures such as latitude band limits that can be applied in post-processing outside of the assimilation experiment. Any key quality choices are detailed in the relevant sections. Full details of the final configuration will be discussed alongside the EDA results in a subsequent report.

3 Modelling instrument noise for simulated HyMS observations

Prior to assimilation in an EDA experiment, simulated hyperMW BTs are perturbed according to the instrument noise characteristics. Here, we use the actual noise measurements, Noise Equivalent Delta Temperature (NEDT) and inter-channel noise correlation values provided by Spire in their pre-launch testing of HyMS. The two components (random and correlated) are described below followed by the steps to generate the perturbations.

3.1 Random component of instrument noise

The instrument noise, NEDT, for microwave sensors is inversely proportional to the channel bandwidth (e.g. from Racette and Lang (2005)). With the large reduction of channel bandwidth for a hyperspectral instrument and practical constraints on compensation from other factors influencing NEDT, a higher noise is therefore expected. Table 2 summarises NEDT estimates for the different HyMS frequency bands. With bandwidths of 6.34 and 40 MHz, values of expected sample NEDT for the temperature- and humidity-sounding bands are 1.6 K and 1.63 K, respectively. These are much higher than the values for broadband sensors, which typically have sample NEDT values on the order of 0.25 K and 0.4 K for these channels, with bandwidths of a few hundred MHz. A pre-requisite for achieving impact with a hyperspectral MW instrument is hence making use of many more channels, to reduce the effective noise through repetitive sampling of similar atmospheric layers from use of several nearby frequencies on HyMS (Maddy et al., 2024).

Additionally, spatial averaging (super-obbing) can be applied to achieve a lower effective noise. This is done, for instance, for ATMS for which observations in three adjacent scan positions and across 3 adjacent scan lines (i.e. 9 fields of view) are averaged together in a 3x3 averaging step (Bormann et al., 2013). This is also adopted in the present work for HyMS. This lowers the effective noise by a factor of three (0.53 K and 0.54 K for temperature- and humidity-sounding channels respectively), assuming that white noise dominates which appears supported from pre-launch characterisation (pers. comm. M. Henry (Spire), 30 Apr 2025). As in previous studies, we mimic the 3x3 averaging by selecting every third observation on every third scanline, without performing explicit averaging, but adopting the lower effective noise values. This approach has an added advantage of introducing further representativeness error in generating realistic BT characteristics especially important for application of the all-sky observation error model.

3.2 Correlated component of instrument noise

In addition to a random element, instrument noise is also correlated between the instrument channels. The values for the HyMS inter-channel noise correlations are summarised in figure 1 (data kindly provided by Spire). For the temperature-sounding channels, correlations between immediately neighbouring channels are more significant with an average value of 0.44, whereas correlations with the next neighbour are only at 0.03. For the humidity-sounding channels which have already been pre-processed into bins of 8 channels, the correlation between these adjacent groups is already small at 0.041 while next nearest neighbours at 0.01. For frequencies further apart than nearest or next nearest neighbours the correlations are negligible and will therefore be neglected in generating the perturbations for the simulated BTs.

3.3 Generation of perturbations

The perturbations applied to the simulated BTs are a combination of the random noise and correlated noise for immediate and next nearest channel neighbours. The steps to do this are as follows:

1. A covariance matrix for the hyperMW instrument is first generated using a product of diagonal matrices containing the random NEDT values, N_{diag}, and a correlation matrix, C (equation 1). The correlation matrix is constructed with diagonal values of one, the first off-diagonals filled with the average correlation value of nearest neighbours and second off-diagonals fille with the average correlation value of next nearest neighbours and all other elements at zero.

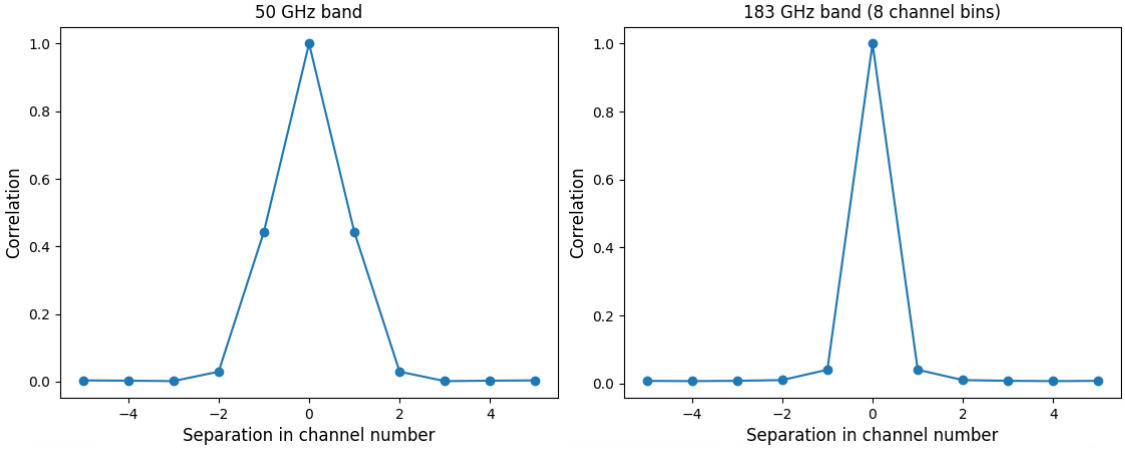

Figure 1: Average correlation of noise between neighbouring channels for the temperature-sounding band (left panel) and humidity-sounding channels after combination into groups of 8 channels (right panel). The position on the x-axis indicates the separation in channel number relative to the central channel of interest.

$$\mathrm{COV} = N_{diag} C N_{diag} \tag{1}$$

2. Random samples from a multivariate normal distribution are taken with a mean of zero and the full covariance matrix provided from step 1 for each instrument channel and generated individually for every space/time location. These values are added to the simulated BTs.

3. These steps are repeated separately for the high-resolution temperature- and humidity-sounding channel blocks. The 89 GHz and three broadband super channels only feature perturbations according to random noise only.

Figure 2 provides a representative example of the simulated BTs for a low peaking high-resolution channel (peak sensitivity around 600 hPa) and the corresponding background departure statistics from a 4D-Var deterministic experiment (see section 2.2 for details on set up). For reference, the BTs and departures around the same frequency on Metop-C AMSU-A 5 are also shown. The large-scale features of the simulated BTs exhibit good agreement to AMSU-A (figure 2, left panels). However, the background departures (figure 2, right panels) reveal a much noisier pattern than AMSU-A. Importantly for the all-sky error model (analysed in depth in section 4) organised features relating to representative errors from cloudy features are still apparent in the hyperMW departures. Similarly, figure 3 shows an example of humidity-sounding hyperMW simulated BTs on a low peaking channel and background departures. The corresponding broadband channel at similar frequency for the MHS instrument is also given. In the case of humidity, representative error tends to dominate so cloud signals remain more apparent above the noise in agreement with the MHS data.

In this process, no attempt is made to model possible systematic biases. We make the assumption that these biases will follow structures already encountered and which are effectively dealt with in the current bias correction scheme. As a new and evolving design that is very different from current MW sensors, there is a possibility that real hyperMW observations will show unfamiliar biases. Techniques to mitigate these may need to be developed in order to allow effective assimilation. Note that further random perturbations are added in the EDA framework, and they are based on the assigned observation error.

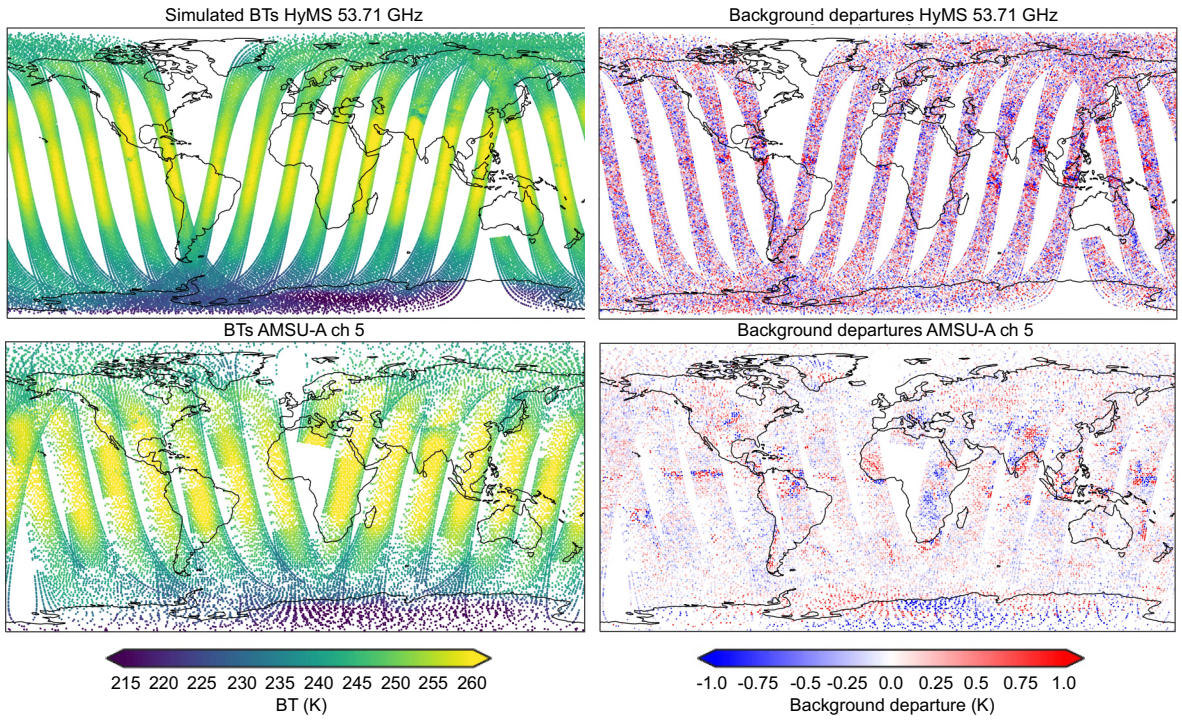

Figure 2: Maps of BT (left column) and background departures (right column) for simulated HyMS data (top row) after perturbations for a frequency around AMSU-A 5 (53.71 GHz) and real AMSU-A 5 data (bottom row) for a single 12h assimilation cycle on 3 June 2024. No quality control is applied.

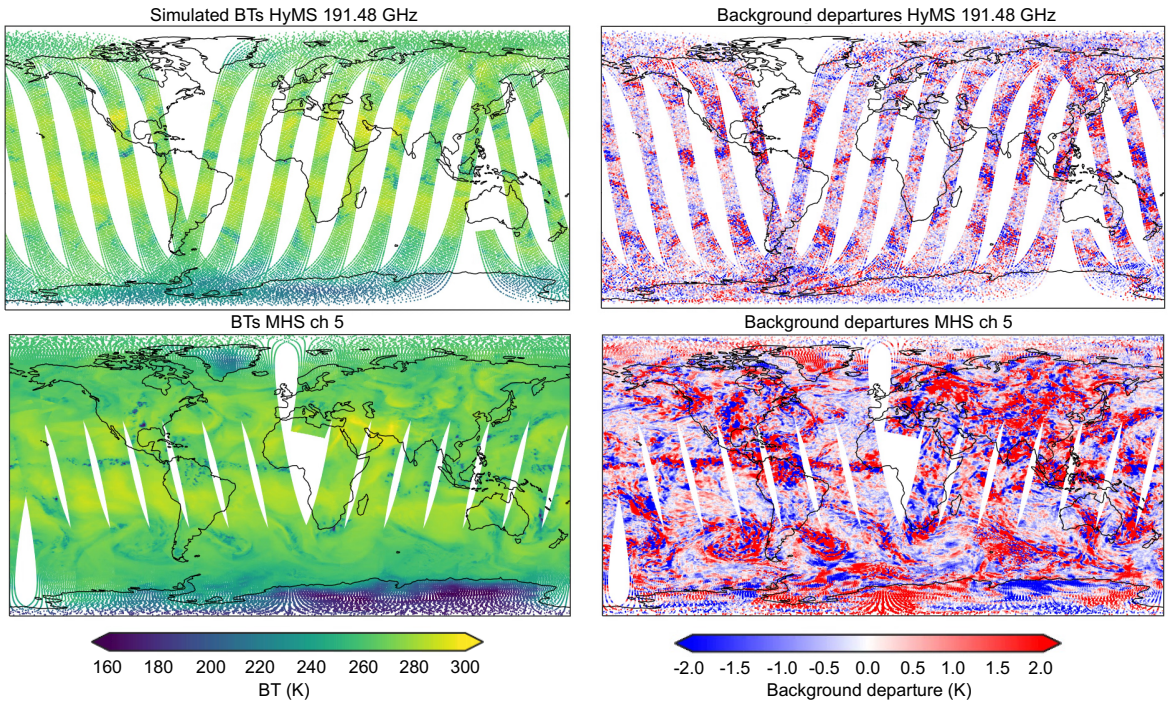

Figure 3: Maps of BT (left column) and background departures (right column) for simulated HyMS data (top row) after perturbations for a very low peaking humidity-sounding channel (191.48 GHz) and real MHS 5 data (bottom row) for a single 12h assimilation cycle on 3 June 2024. No quality control is applied.

4 Adaptation of the all-sky observation error model

As for existing MW sensors, the simulated BTs from a hyperMW instrument will be assimilated through the all-sky scheme (Geer et al., 2010, 2017). Therefore, accompanying observation errors will be treated by the all-sky error model where observation errors are larger in the presence of cloudy signals either from the model or observations (Geer and Bauer, 2011). This situation dependence accounts for different representativeness of cloud in the model and observations. The success of the all-sky model is reliant on indicators that can adequately estimate the cloudy signals in the affected frequencies. Additionally, it requires suitable definition of minimum error values, applied in clear-sky situations, and maximum error values, applied where the cloudy signal saturates. In this section, a summary of the key aspects of the all-sky observation error model is first presented, based on the detailed discussion found in Geer et al. (2014). Adaptation of the configuration for existing sensors to suit the HyMS instrument is discussed, focusing on the choice of cloud indicators and a method to define clear-sky and saturated-cloudy parameters.

4.1 Introduction to the all-sky observation error model

The all-sky observation model used at ECMWF is formulated in terms of a cloud indicator, as illustrated in the simple schematic in figure 4. There are two indicators for the long established AMSU-A instruments. Over land the difference 23.8-89 GHz provides a scattering index which exploits the increased scattering from frozen hydrometeors at 89GHz compared to 23.8GHz (Bennartz et al., 2002). Over ocean, the predictor is the retrieved liquid water path (Grody et al., 2001) which is derived from 23.8 GHz and 31.4GHz channels. More recently, assimilation of the Arctic Weather Satellite (AWS) which does not have the lower frequencies (less than 50 GHz) accommodated has required a different approach. Instead, BTs from a single channel are used where cloudy signals are extracted from the window channel at 52.8 GHz (Duncan et al., 2025). This follows an approach previously suggested by Okamoto et al. (2014) for all-sky assimilation of infrared radiances. Earlier work showed that this single channel formulation performs similarly to the AMSU-A indicators and was also successfully used in earlier simulated satellite studies (Lean et al., 2021, 2025).

For humidity sounding channels, the corresponding error model utilises channels at 89GHz and 150GHz to form the cloud indicator (Geer et al., 2014). Differences in scattering from precipitation-sized ice particles are exploited, similar to the current land scattering index model for temperature sounding channels. This makes it very suited to the 183GHz channels where frozen particles dominate the scattering (Lui, 2008; Geer and Baordo, 2014).

The cloud indicator used in the error model is formulated by taking the average (leading to the term "symmetric cloud indicator") of the cloud indicator values for the observations and the model background:

$$C_{SYM} = (P_{obs} + P_{bkrd})/2 \tag{2}$$

Where P_{obs} is the indicator calculated using observed values e.g. the difference in observed brightness temperatures at 23.8 and 89 GHz for the scattering index and P_{bkrd} is calculated using the model background equivalent brightness temperatures. The final observation error is then constructed with either a linear or quadratic dependence on the cloud indicator as the following (reproduced in the linear form using the same notation from Geer et al. (2014)):

$$g_{clr} \in C_{SYM} <= C_{clr} \tag{3}$$

$$g(C_{SYM}) = g_{clr} + (g_{cld} - g_{clr}) \left(\frac{C_{SYM} - C_{clr}}{C_{cld} - C_{clr}} \right) \in C_{clr} < C_{SYM} < C_{cld} \tag{4}$$

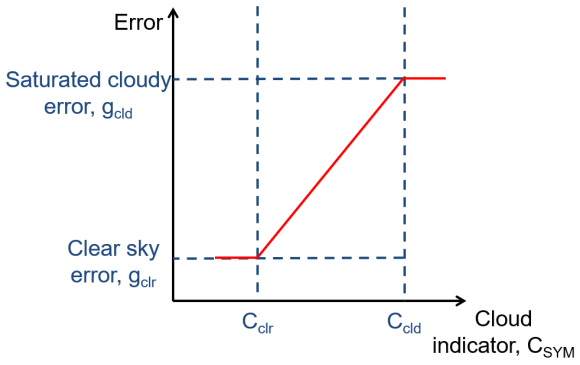

Figure 4: Simple schematic showing how the coefficients in equations 3 - 5 define the form of the error model.

$$g_{cld} \in C_{SYM} >= C_{cld} \tag{5}$$

Where g_{clr} and g_{cld} are the clear sky and saturated cloudy error values respectively while C_{clr} and C_{cld} are threshold values of the symmetric cloud indicator to separate clear and saturated cloudy situations, respectively. The clear sky values reflect the individual channel noise estimates of the instrument, inflated in recognition of other error sources e.g. from forward modelling error. In the case of temperature-sounding channels, the instrument noise is the principal contribution to the minimum error while for humidity-sounding channels, sensitive to the water vapour spectrum, representative errors are dominant factor. The cloudy saturation value and the choice of a linear or quadratic nature of the model are determined by analysing the standard deviation of background departures binned as a function of the symmetric cloud indicator. These values are determined separately for each satellite and individual instrument channels. Figure 4 illustrates how the coefficients define the construction of the error model.

Currently AMSU-A channels 5 - 9 all use this error model to increase errors in cloudy situations (Duncan et al., 2022). As the channel number increases, the height of the peak sensitivity also increases (with AMSU-A 9 most sensitive around 80-90 hPa) and correspondingly the impact of cloud decreases. This means that the difference between the clear sky (g_{clr}) and saturated cloudy values (g_{cld}) gradually reduces with increasing channel number. For channel 10 and above, with little sensitivity to the troposphere, the impact of cloud is negligible so the error model becomes a constant value given by g_{clr}. All MHS channels are treated with situation dependent errors (Geer et al., 2014).

4.2 Proposed cloud indicators for HyMS

The HyMS instrument does not have all the frequencies available that are currently used for cloud indicators for the long-established MW instruments (i.e. no low frequencies or 150 GHz). Instead, the 52.8 and 190.32 GHz super channels will be used to construct a cloud indicator for temperature- and humidity-sounding channels respectively, following approaches that have been previously adopted for the infrared (Okamoto et al., 2014) or the assimilation of AWS data (Duncan et al., 2025; Lean et al., 2026a). The cloud indicator is based on BTs of a single channels and expressed as:

$$C_{single} = (\text{abs}(BT_{obs} - BT_{bkclr}) + \text{abs}(BT_{bkcld} - BT_{bkclr}))/2 \tag{6}$$

Here, the cloud effect in the observation is estimated by taking the absolute difference between the actual observations, BT_{obs}, and the simulated clear sky brightness temperature from the model background (BT_{bkclr}). The cloud effect in the model background can be expressed as the absolute difference between the equivalent brightness temperature from the model background using the cloudy radiative transfer model, BT_{bkcld}, and the clear sky calculation for the same model background (BT_{bkclr}). While this type of cloud indicator has not yet been used operationally for 183 GHz channels, investigations with current sensors suggest that the impact of the data is very similar compared to use of the scatter index parameter usually used (pers. comm. S. Panditharatne, Jan 2026).

A key characteristic of a successful cloud indicator is to characterise well the larger representation errors associated with cloudy situations, reflected in larger standard deviations of background departures. In clear-sky situations, as indicated by low values of C_{single}, standard deviation of background departures is expected to be low in the absence of the larger representativity errors from cloud. As a higher presence of cloud is estimated (in either model or observations) by increasing C_{single}, the standard deviation is also expected to rise. Eventually, a point at high values of C_{single} - cloudy saturation - can be reached where the standard deviation no longer increases as representativity errors plateau. The simulated BTs are required to hold these characteristics to enable effective assimilation in the all-sky scheme.

Figure 5 shows examples of the standard deviation of background departures/cloud indicator relationship for three channels with peak sensitivities similar to AMSU-A channels 5 - 7. For lower peaking temperature-sounding channels (figure 5, left panel) there is a clear dependence of standard deviation versus cloud indicator as required. The value range of the cloud indicator and standard deviation is similar to those seen when using real AMSU-A data (e.g. see analysis in Lean et al. (2021)). For higher peaking temperature-sounding channels, the cloud signals are small relative to the instrument noise on HyMS (0.53 K, table 2). For instance, at frequencies with peak sensitivity around 250 hPa, similar to AMSU-A channel 7, the cloudy signals of the simulated HyMS data are no longer distinguishable (figure 5, right panel). This means that a constant observation error value is sufficient for these channels. This is again consistent with the experience from AMSU-A, where the maximum error assigned to cloudy observations is smaller than the HyMS effective noise.

Similarly, examples from high, middle and low peaking humidity-sounding channels are shown in figure 6. Now the NEDT is small compared to the representativity errors, all channels exhibit a clear dependence of standard deviation on the cloud indicator. For higher peaking channels, there is a bump in the trend where the rise in standard deviation slows before increasing again at low cloud indicator values around 1-2K e.g. figure 6, left panel. This is also seen in real MW data when using the single channel indicator but not present using the original scatter index formulation (not shown). For very low indicator values, both observation ($BT_{obs} - BT_{bkclr}$) and background ($BT_{bkcld} - BT_{bkclr}$) contributions must be small. While the latter term correctly identifies cloud contributions in the model background, the former will also be affected by errors in the clear-sky background as well as noise in the observations. Situations where errors in the background are small for the indicator channel are likely to correlate with low errors in the high-resolution 183 GHz and therefore lead to small standard deviation just due to selective sampling. In addition, some clear-sky humidity features are poorly captured due to suboptimal modelling of both gravity waves and filaments of water vapour. These could result in significant variation in background departures while maintaining a low indicator value. This highlights a limitation in the design a of single channel indicator that applies to both temperature- and humidity-sounding channels. When relying purely on the background departure statistics, careful thought is required for estimating the minimum clear-sky g_{clr} to avoid underestimation of errors. A small positive value as a lower limit could be appropriate for the minimum cloud indicator value, C_{clr}. The setting of the parameters is addressed in the next section.

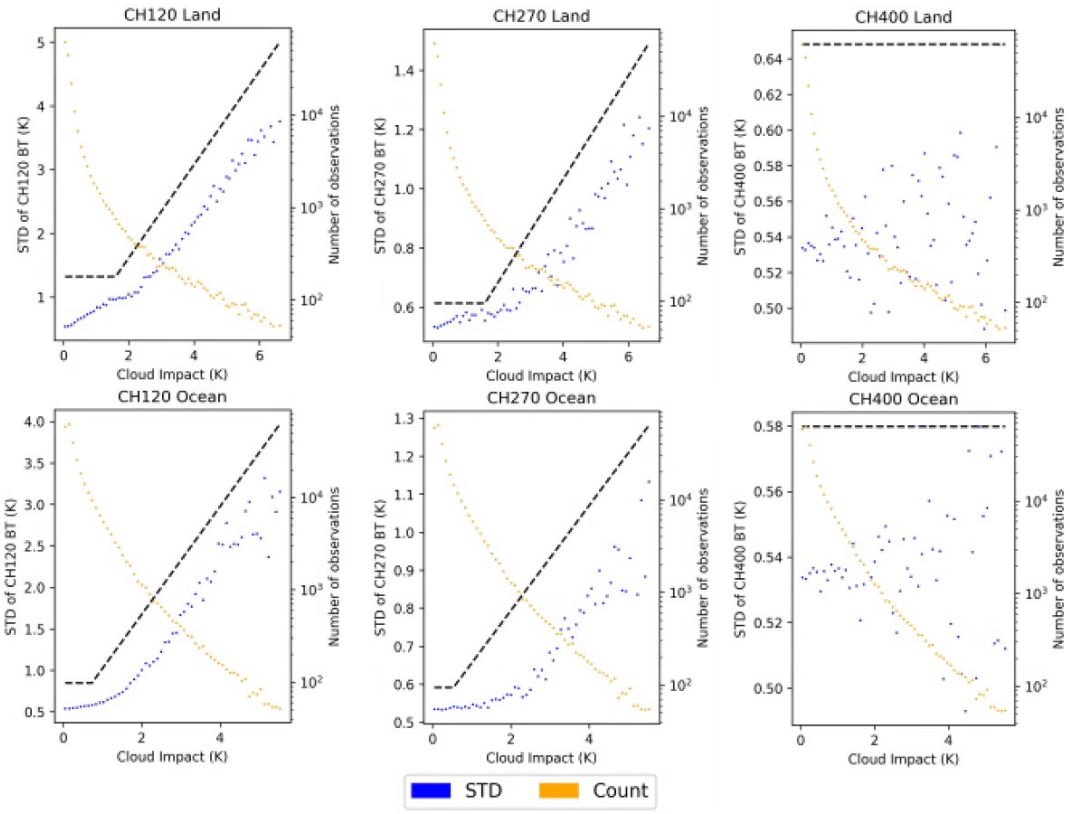

Figure 5: Standard deviation of observation - background departures for simulated temperature-sounding HyMS channels binned as a function of the symmetric cloud indicator using a super channel at 52.8 GHz. Dashed black line shows the estimated error model fit as discussed later in section 4.3.2. Top row shows land points and bottom row shows sea points. Columns (from left to right) are for channels at frequencies 53.74, 54.47 and 55.10 GHz, around the frequencies covered by AMSU-A 5, 6 and 7 respectively. Crosses indicate the number of observations in each bin. Data are from 3-14 Jun 2024, limited to $\pm$60N to exclude sea ice contamination and no quality control has been applied.

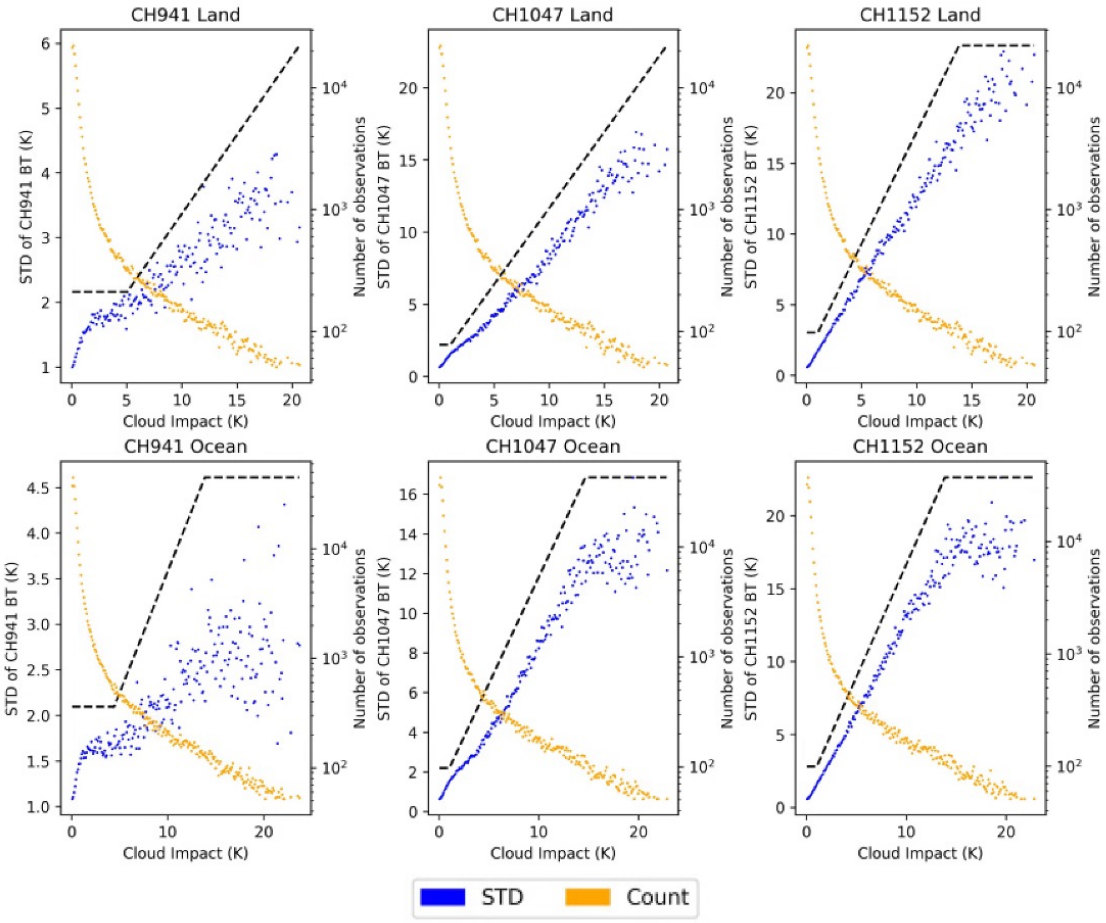

Figure 6: As for figure 5 but columns (left to right) correspond to humidity-sounding channels around the beginning, middle and end of the band at 183.49, 189.87 and 191.48 GHz respectively.

4.3 Automating all-sky error model parameter definition

Prior to assimilation, the all-sky observation error model requires definition of parameters for the clear-sky minimum and saturated-cloudy maximum (as illustrated in figure 4). For existing MW data, these values are tuned empirically for each frequency and satellite, based on background departure statistics (similar to those discussed above). While this can be done for a satellite with a small number of channels, it is not practical to scale such an empirical technique to a hyperMW instrument. Estimates for the minimum and maximum errors in earlier studies with simulated MW data, where proposed instruments shared a lot of characteristics with existing MW sounders, were closely linked to values used for real data (Lean et al., 2025). However, with the design of HyMS being so different from conventional sensors, especially with the higher instrument noise, extending the same links may not be appropriate. Instead, we propose a more automated approach based on standard deviation of background departures generated from a deterministic 4D-Var experiment.

4.3.1 Method for automating parameter calculation

A method is currently in development at ECMWF which better automates parameter estimation for the all-sky observation error model. It aims to create a more robust and faster process for obtaining values while being flexible and easily adaptable to use on existing MW sensors as well as future instruments such as HyMS. The relationship between the standard deviation of background departures and cloud indicators forms the basis of the analysis (similar to the examples earlier in figure 5 and 6). A linear regression is fitted to obtain initial values for the minimum and maximum values of error (g_{clr} and g_{cld} respectively) and cloud indicator (C_{clr} and C_{cld} respectively). This fitting takes into account the presence of features such as a plateau in the standard deviation for large cloud indicators and deviations from a linear relationship at low indicator values e.g. as discussed earlier regarding figure 6, left panel. To avoid assigning errors that are too small, and in line with the typical values currently used for MW sounders, the estimates from the line fitting are inflated to produce more conservative error values. The magnitude of the inflation is allowed to vary to suit the characteristics of the different frequencies. Development is still ongoing and further updates to the scheme are possible. A summary of the details of the derivation in its current form is given in Appendix A.

4.3.2 Preliminary parameters derived for HyMS

Using the automated approach, parameters needed for the observation error model have been generated for channels on the HyMS instrument. Figure 5 shows the resulting error model given in the dashed line fitted to a selection of temperature-sounding channels situated close to the frequencies of AMSU-A 5-7. The clear dependence of standard deviation of background departure on the cloud indicator allows sensible derivation of observation error model parameters. For frequencies on HyMS close to AMSU-A channel 7 (peaking around 250hPa), the automated derivation correctly identifies no significant rise in standard deviation and assigns a constant error value. This means that situation dependent errors are applied to a smaller frequency range than currently used with existing MW sensors. However, the cloudy signals in the broadband instruments are small at these higher peaking channels. As an expected consequence from the higher instrument noise, the estimated minimum clear-sky errors are larger for HyMS than AMSU-A, e.g. 0.60 K and 0.17 K respectively for frequencies around 54.4 GHz (AMSU-A 6) over ocean.

Representative examples of the error model fitting across the 183 GHz frequency band are shown in figure

6. For the higher peaking channels, the error model adjusts for the hump feature at low cloud indicator values, setting minimum clear-sky errors around 2-2.5 K. This is similar to the operationally used values for current sensors which are typically around 1.8-2.2 K. The dominance of the representative errors in the clear-sky means that despite the higher instrument noise, the estimates for HyMS are comparable to existing sensors.

To achieve sensible minimum and maximum error estimates from the automated process, the inflation levels employed here are initially tuned based on experience with existing MW sensors. However, the scheme can be adapted if required to apply higher or lower levels of inflation. In particular, adjustment may be required depending on the strategy for dealing with the inter-channel errors correlations on a hyperspectral MW instrument. Correlations could be handled explicitly with defined observation error correlation matrices or implicitly by inflating the errors of a diagonal observation error matrix. As part of the next phase in this project, sensitivity experiments using different observation error values will be run in order to assess the impact of the two strategies and influence of error inflation. Earlier work considering the impact of varying NEDT suggested that changes in the clear-sky minimum error, where data counts are highest, can significantly impact the EDA spread (Lean et al., 2026b).

5 Accounting for inter-channel error correlations

In the all-sky assimilation of MW instruments at ECMWF, observation errors are currently assumed to be diagonal, and any observation error correlations are neglected. Observation error correlations can arise, for instance, from representation errors linked to the forward modelling of clouds or differences in spatial scales. Error correlations can also arise from correlations in the instrument noise, as noted earlier for HyMS. Traditionally, observation errors have incorporated some inflation to mitigate against negative impacts in assimilation from the unspecified error correlations (Geer, 2019). For the clear-sky assimilation of infrared instruments, however, inter-channel error correlations are taken into account, and this has led to significantly improved forecast impact (e.g., Bormann et al., 2016; Weston et al., 2014). Similar approaches have also been adopted for the clear-sky assimilation of ATMS (e.g. Weston and Bormann, 2018).

Observation error correlations encountered in all-sky assimilation can be considerably situation-dependent, reflecting the different characteristics of representation error in clear and cloudy situations. Figure 7 gives an estimate of the error correlations present in the case of HyMS, for two situations over sea, one representing clear-sky conditions, and one representing cloudy conditions. The estimate is based on background departures taken from a 4D-Var experiment assimilating simulated HyMS data, in a similar way as used to derive the parameters to model the observation error standard deviations described above. These statistics are necessarily affected by contributions from background errors, and alternatively other approaches could be employed to ameliorate this, such as the Desroziers diagnostic (Desroziers et al., 2005). As can be seen, for clear-sky conditions, inter-channel error correlations are small for the temperature-sounding band, and they are mostly restricted to the first off-diagonal channel pairs (figure 7, top panel). This reflects the dominant contribution from the instrument noise for these channels, including the inter-channel noise correlations noted earlier. In contrast, considerable error correlations are present for the 183 GHz channels (channels 941 and above). Higher error correlations for humidity-sounding channels have been noted before for clear-sky assimilation, for instance for IASI or ATMS, and they are thought to arise from spatial representativeness errors (e.g., Weston and Bormann, 2018; Bormann et al., 2016; Weston et al., 2014). Much stronger error correlations are found for the cloudy category (figure 7, bottom panel), with significant blocks of correlations for the lowest temperature-sounding channels as well as the humidity-sounding channels. In addition, there are cross-

correlations between these blocks of channels. All of these blocks of correlations are largely the result of representation errors relating to cloud modelling, affecting a range of channels in a similar way.

Taking such inter-channel error correlations into account for all-sky assimilation is an active area of research. Recently, the technical capability to explicitly account for inter-channel error correlations for the all-sky assimilation of MW sounders has been added in the ECMWF system (Steele et al., 2025). This includes two key aspects: 1) the capability to take the situation-dependence of the error correlations into account. This is done using a look-up-table approach that selects pre-defined correlation matrices based on the values of the symmetric cloud indicators already used in the observation error model. 2) the capability to account for inter-channel observation error correlations in combination with Variational Quality Control (VarQC, Andersson and Järvinen, 1998). VarQC estimates the probability of gross error during the assimilation and down-weights the observations accordingly. This is considered an important element of the all-sky assimilation of MW radiances, as it protects against gross representation errors in the modelling of clouds. Testing has so far been limited to ATMS, and the forecast impact from accounting for these error correlations was found to be small compared to the overall impact of the assimilation of ATMS data. The largely neutral impact is in contrast to the findings with clear-sky assimilation of infrared or microwave data noted earlier. As VarQC is not used in the clear-sky assimilation, a possible reason may be that VarQC is already performing situation-dependent down-weighting of observations in a broadly similar way as achieved through taking inter-channel error correlations into account. Further details on the developments on taking into account error correlations for all-sky assimilation of MW observations can be found in Steele et al. (2025).

While the experiments with ATMS provide some indication that taking inter-channel error correlations into account is less important for all-sky MW assimilation of traditional MW instruments, it is an open question whether this extends to assimilating several hundreds of channels as in the case of HyMS. To test the sensitivity of our impact evaluations to the specification of error correlations, we hence aim to adopt the technical framework developed by Steele et al. (2025) and apply it to HyMS. When taking into account the inter-channel error correlations, the specification of the error variances stays unchanged and follows the approach described in the previous section. The situation-dependence of the error correlations is taken into account through a look-up-table approach, using suitably chosen bins of the symmetric cloud indicator introduced above. As we use two different cloud indicators for HyMS (based on the 52.8 and 190.32 GHz channels), we adopt a 2-dimensional look-up-table, as in Steele et al. (2025). The number of bins used is a trade-off between detailed modelling of the situation-dependence and adequate sampling to specify the required matrices in a robust way. Steele et al. (2025) made the pragmatic choice to use three bins for each cloud indicator, broadly reflecting “clear”, “weakly cloudy” and “strongly cloudy” conditions, and these were shown to broadly cover main correlation characteristics. We take a similar approach here, resulting in a 3x3 look-up-table with nine matrices. Table 3 gives the values for the boundaries of the cloud indicator bins envisaged for HyMS, over sea and land, respectively. The choices have been adopted from experiments with all-sky assimilation of ATMS. While they have been found to also provide a pragmatic representation of leading changes in the correlation structure for HyMS, the choice of boundaries may be subject to refinement. Interpolation between the correlation matrices could be considered, but this will be left for future refinements.

6 Summary

HyperMW instruments present a significant change in design from the heritage MW sounders. This study aims to evaluate the benefit of a hyperMW instrument to global NWP in order to assist in recommendations for shaping the future MW constellation. Here, we build on the simulation framework and

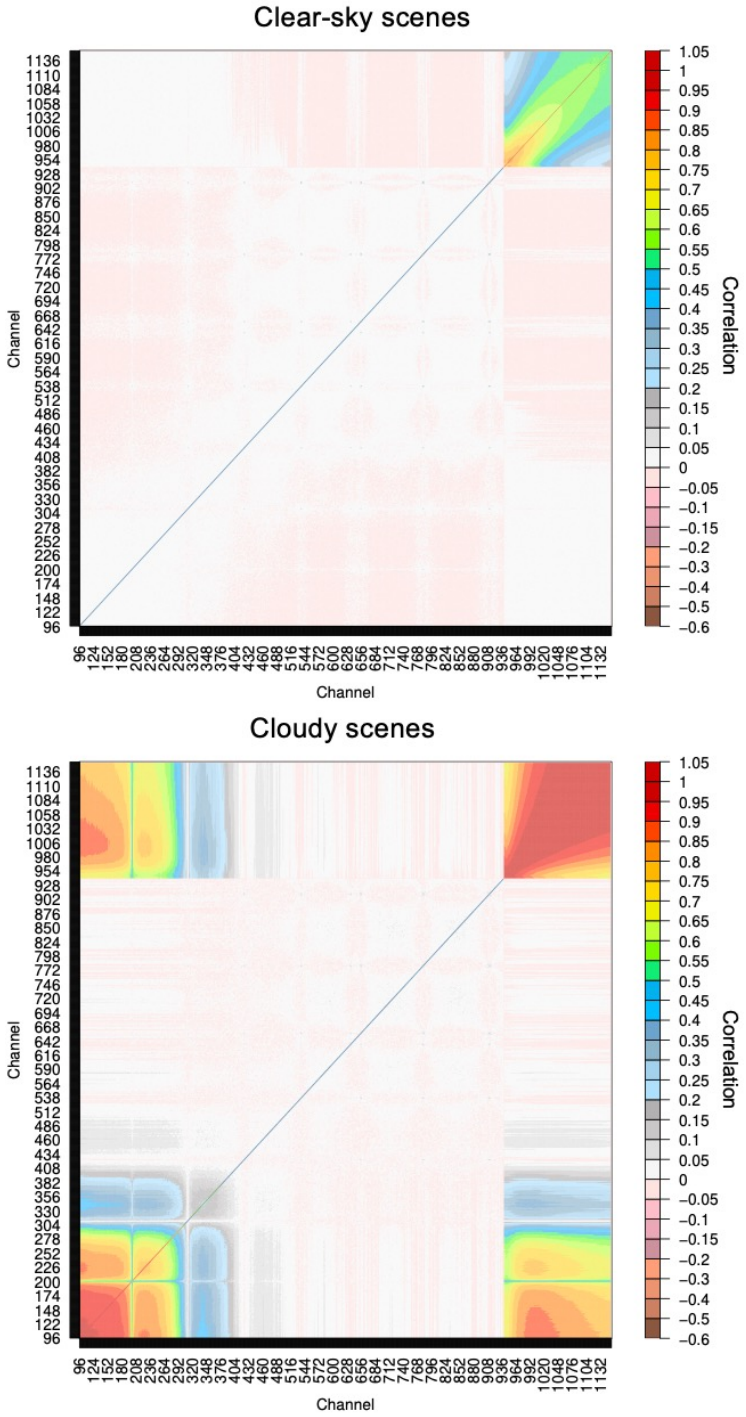

Figure 7: Inter-channel correlations of background departures over sea for the HyMS channels considered for assimilation in this study. Statistics have been derived over the period 2 – 14 June 2024 from a 4D-Var experiment with simulated HyMS data, based on all used observations. Two different situations are shown: Clear sky (top panel), that is, $CI_{52.8\ GHz} < 0.5$ K and $CI_{190.32\ GHz} < 1$ K, and strongly cloudy (bottom panel), $CI_{52.8\ GHz} > 0.5$ K and $CI_{190.32\ GHz} > 4$ K. Channels 1-939 correspond to the temperature-sounding band and channels 941-1152 correspond to the humidity-sounding band.

Table 3: Boundaries for the cloud impact parameter bins used for the representation of error correlation matrices for HyMS.

Cloud indicator	Bin boundaries [K] over sea	Bin boundaries [K] over land
$CI_{52.8\ GHz}$	0.0, 0.5, 2.5, 8.0	0, 0.5, 3, 8.0
$CI_{190.32\ GHz}$	0, 1, 4, 80	0, 1, 4, 80

application of the EDA method used in previous future MW instrument studies (Lean et al., 2026b, 2025) to assess the impact. The HyMS instrument forms the basis of the hypothetical sounder to be investigated. Full use of the high-resolution channels is proposed to maximise the potential information content but with relatively conservative geographical screening, such as limiting surface sensitive channels, following the current MW sounder use. Achieving realistic results from the EDA technique is reliant on an appropriate assimilation strategy for the new data and an adequate representation of the observation uncertainties. The latter has been the focus of this report, discussing the generation of initial perturbations to the simulated observations and strategies for defining the observation errors. Key concepts have been presented and ongoing testing, particularly using experiments to assess the sensitivity of the impact to the observation error settings, will inform the final configuration.

The modelling of the instrument noise for the simulated hyperMW BTs includes random and correlated components based on pre-launch measurements from the real HyMS instrument. After mimicking a super-obbing step (averaging together nine fields of view), the random noise is based on sample NEDT values of 0.53 and 0.54 K for the temperature- and humidity-sounding bands respectively. Correlations in the noise are defined only for the nearest and next nearest neighbours as they quickly become negligible for channels that are further apart. Perturbations for the simulated BTs are generated by taking random samples from a multivariate normal distribution with a mean of zero and covariance matrix constructed by the associated correlation matrix and variances provided by the NEDT values.

The hyperMW instrument will be assimilated in the all-sky framework and therefore use an adapted version of the observation error model used for current MW sounders. Three significant aspects have been considered:

1. Defining appropriate indicators of cloudy signals that capture the larger representation errors in cloudy scenes, i.e. the standard deviation of background departures increases with greater presence of cloud estimated by the indicator.
2. Generating parameters required for the all-sky error model which include the minimum clear-sky and maximum saturated-cloudy errors for each channel
3. With the large increase in channels, inter-channel error correlations may have a more significant influence than current MW sounders. Although not yet operationally used, the recently available technical framework for explicit definition is explored.

Following success in operational use and earlier simulated MW data studies (Duncan et al., 2025; Lean et al., 2026a), indicators using single, low peaking channels at 52.80 and 190.32 GHz are proposed for the temperature and humidity bands respectively. The channels used in the indicator are low-noise super channels constructed from averaging a large number of high-resolution channels to approximate channels on current sensors (roughly equivalent to AMSU-A channel 4 and MHS channel 5). The simulated hyperMW BTs display a good dependence of standard deviation of background departure on

these indicators as required. However, where NEDT is a dominant factor in the observation error for the temperature-sounding channels, the small cloud signals relative to the instrument noise means that a relationship cannot be detected for channels peaking in the upper troposphere.

The observation error model parameters are derived using a new automated approach, replacing a previous manual approach. The standard deviation of background departure/cloud indicator relationship is analysed using a linear regression technique. This accounts for the potential plateau in standard deviation at high cloud indicator values. Minimum and maximum error settings incorporate an inflation factor to ensure a more conservative estimate that avoids observation errors that are too small leading to potential detrimental impacts on the assimilation system. Development initially focused on real MW data and tuning to achieve the final settings for the hyperMW instrument is ongoing.

The technical capability to assimilate MW sounders with explicit definition of correlated inter-channel observation errors was initially developed for ATMS (Steele et al., 2025) but is adapted for application to a hyperMW instrument. Significant inter-channel correlations are diagnosed in the simulated BTs, particularly in cloudy scenes, for channels with high cloud sensitivity. Channels are especially affected within the humidity band and low peaking temperature-sounding channels but also with significant inter-band correlations between the same humidity and temperature-sounding channels. The scheme categorises situations as being clear, weakly cloudy or strongly cloudy with the boundaries on the cloud indicator being chosen empirically. This results in nine correlation matrices that can be used as a look-up table for assimilation. Preliminary settings for the boundaries on the cloud indicator have been used here and may be subject to refinement.

The definition of uncertainties for the new hyperspectral technology relies on recent and still evolving developments for the setting of the error model parameters and the explicit inclusion of inter-channel errors correlations. To determine the final settings for assimilation of the simulated BTs, the next step will be to design and run EDA sensitivity experiments. It is important to gauge the magnitude of changes to the expected impact in response to adjustments to the error model. In particular, understanding the role of error inflation compared to using the new correlated error scheme. Once the final assimilation settings are confirmed, EDA experiments will be carried out that fully explore the benefits of a hyperMW instrument with context from real MW sensors.

Acknowledgements

The authors would like to thank Mohammed Belal, Manju Henry and Vlad Irisov at Spire who kindly provided the details for HyMS. The authors would also like to gratefully acknowledge Liam Steele for all his work on developing the capability and continued support on using inter-channel error correlations in the all-sky framework. Thanks also to David Duncan and Alan Geer for their valuable advice on the parameter setting in the observation error model.

Appendix A Strategy for automation of all-sky error model parameters

A method to automate the derivation of parameters for the all-sky observation model is currently under development at ECMWF. This will enable a more efficient and robust process compared to the current empirical approach, that can also be easily scaled to the hundreds of channels on a hyperMW instrument. The key outputs are the minimum and maximum values of error, g_{clr} and g_{cld} respectively, and cloud indicator, C_{clr} and C_{cld} respectively (as shown in the simple representation in figure 4). The standard

deviation of background departures, produced from a deterministic 4D-Var experiment, forms the basis for the analysis. The standard deviation values are first binned as a function of cloud indicator, and the relationship is investigated. A linear regression is fitted to the binned data which provides the initial estimates for the error model parameters. The line fitting is carried out while accounting for deviations from a linear trend, such as a plateau in the standard deviation for large cloud indicator values. The following gives an overview of the current steps, based on the single channel cloud indicator formulation, to derive the error model parameters, noting that some details may be subject to change before a final version is confirmed:

C_{cld}: If a plateau in standard deviation of background departures at high cloud indicator values is detected, C_{cld} is set at the plateau point. If no plateau is present, possibly due to an insufficiently large data sample, C_{cld} is simply assigned the largest value in the data set.

C_{clr}: Here, deviations are considered from a linear relationship and incorporating an awareness of unreasonably low standard deviation values, as an artifact of the single channel cloud indicator formulation (e.g. as seen in figure 6). Where appropriate, C_{clr} is set to a low positive value to reflect clear-sky situations applying to a small range of cloud indicator values starting from zero. In the case of e.g. higher peaking temperature-sounding channels with less sensitivity to the clear-sky water vapour features in the troposphere, C_{clr} is set to zero.

g_{clr}: rather than directly using the intercept from the line regression output, the clear-sky error is subject to inflation. If $C_{clr} > 0$, then g_{clr} is the standard deviation value, estimated at C_{clr} i.e. neglecting potentially spuriously low standard deviation values. If C_{clr} is set to zero, the factor for the error inflation is dependent on the uncertainty in the line fitting, which provides an estimate of the quality of the standard deviation/cloud indicator relationship. This aims to produce a more conservative estimate of the error, in line with current operational values that are inflated e.g. to indirectly account for error correlations.

g_{cld}: the estimation of the maximum error values uses parameters from the linear regression, g_{clr}, C_{clr} and C_{cld}, and also an inflation factor to ensure errors are not underestimated. Similar to g_{clr}, the inflation is tied to the uncertainty in fitting the standard deviation/cloud indicator relationship. In order to maintain adequate levels of inflation, there is a further variable scaling factor applied to the uncertainty. This avoids cases where a large uncertainty in the line fitting, such as with the noisier temperature-sounding channels on HyMS results in inflation that is unreasonably conservative.

In the case where no relationship between standard deviation of background departure and cloud indicator is detected (using a threshold on the variation in the standard deviation of background departures across all cloud indicator values), the observation error for that channel is set to a constant value. This constant is chosen as equal to the largest binned value of standard deviation of background departure.

References

Andersson, E., Järvinen, H.J., 1998. Variational quality control. ECMWF Technical Memorandum , 31ppdoi:10.21957/lqz2wn16g.

Atkinson, N., 2015. NE△T specification and monitoring for microwave sounders. NWP SAF Technical Report, version 1.1 Doc ID: NWPSAF-MO-TR-033, 12pp.

Bennartz, R., Thoss, A., Dybbroe, A., Michelson, D., 2002. Precipitation analysis using the Advanced Microwave Sounding Unit in support of nowcasting applications. Met. Apps , 177–189doi:https://doi.org/10.1017/S1350482702002037.

Bormann, N., Bonavita, M., Dragani, R., Eresmaa, R., Matricardi, M., McNally, A., 2016. Enhancing the impact of iasi observations through an updated observation-error covariance matrix. Quarterly Journal of the Royal Meteorological Society 142, 1767–1780. doi:https://doi.org/10.1002/qj.2774.

Bormann, N., Fouilloux, A., Bell, W., 2013. Evaluation and assimilation of atms data in the ecmwf system. Journal of Geophysical Research: Atmospheres , 12,970–12,980doi:https://doi.org/10.1002/2013JD020325.

Desroziers, G., Berre, L., Chapnik, B., Poli, P., 2005. Diagnosis of observation, background, and analysis-error statistics in observation space. Q. J. R. Meteorol. Soc. 131, 3385–3396.

Duncan, D.I., Bormann, N., Dahoui, M., Crepulja, M., 2025. Assessment of the Arctic Weather Satellite in NWP. EUMETSAT contract RFQ/21/1383948 URL: https://www.ecmwf.int/en/elibrary/81681-assessment-arctic-weather-satellite-nwp, doi:10.21957/232efc59cf.

Duncan, D.I., Bormann, N., Geer, A.J., Weston, P., 2022. Assimilation of AMSU-A in All-Sky Conditions. Monthly Weather Review 150, 1023 – 1041. doi:10.1175/MWR-D-21-0273.1.

Gambacorta, A., Piepmeier, J., Stephen, M., Santanello, J., Blaisdell, J., Moradi, I., McCarty, W., Rosenberg, R., Kotsakis, A., Gambini, F., Mohammed, P., Kroodsma, R., MacKinnon, J., Adams, I., Racette, P., 2023. Advancing atmospheric thermodynamic sounding from space using hyperspectral microwave measurements. IEEE Journal of Selected Topics in Applied Earth Observations and Remote Sensing 16, 5204–5218. doi:10.1109/JSTARS.2023.3269697.

Geer, A., Ahlgrimm, M., Bechtold, P., Bonavita, M., Bormann, N., English, S., Fielding, M., Forbes, R., Hogan, R., Hólm, E., Janiskova, M., Lontiz, K., Lopez, P., Matricardi, M., Sandu, I., Weston, P., 2017. Assimilating observations sensitive to cloud and precipitation. ECMWF Technical Memorandum No.815. doi:10.21957/sz7cr1dym.

Geer, A., Baordo, F., Bormann, N., English, S., 2014. All-sky assimilation of microwave humidity sounders. ECMWF Technical Memorandum No. 741, 57pp. doi:10.21957/obosmx154.

Geer, A., Bauer, P., Lopez, P., 2010. Direct 4D-Var assimilation of all-sky radiances. Part II: Assessment. ECMWF Technical Memorandum No.619.

Geer, A.J., 2019. Correlated observation error models for assimilating all-sky infrared radiances. Atmospheric Measurement Techniques 12, 3629–3657. doi:10.5194/amt-12-3629-2019.

Geer, A.J., Baordo, F., 2014. Improved scattering radiative transfer for frozen hydrometeors at microwave frequencies. Atmos. Meas. Tech. 7, 1839–1860.

Geer, A.J., Bauer, P., 2011. Observation errors in all-sky data assimilation. Q. J. R. Meteorol. Soc. 137, 2024–2037. doi:doi:10.1002/qj.830.

Grody, N., Zhao, J., Ferraro, R., Weng, F., , Boers, R., 2001. Determination of precipitable water and cloud liquid water over oceans from the NOAA 15 advanced microwave sounding unit. J. Geophys. Res. , 2943–2953doi:doi:10.1029/2000JD900616.

Harnisch, F., Healy, S.B., Bauer, P., English, S.J., 2013. Scaling of GNSS Radio Occultation Impact with Observation Number Using an Ensemble of Data Assimilations. Mon. Wea. Rev. 141, 4395–4413. doi:doi:http://dx.doi.org/10.1175/MWRD-13-00098.1.

Henry et al., 2023. Development of a hyperspectral microwave sounder for enhanced weather forecasting, in: IGARSS 2023 - 2023 IEEE International Geoscience and Remote Sensing Symposium, pp. 1092–1095. doi:10.1109/IGARSS52108.2023.10282436.

Hocking et al., 2025. Rttov v14 science and validation report. RTTOV online documentation NWPSAF-MO-TV-051 Version 1.0.1. doi:https://nwp-saf.eumetsat.int/site/download/documentation/rtm/docs_rttov14/rttov14_svr.pdf.

Ishibashi, T., 2024. Accurate global atmospheric state analysis using objective error statistics including observation error dependence on water substance field. Earth and Space Science 11, e2023EA003029. doi:doi:10.1029/2023EA003029.

Janjic, T., Bormann, N., Bocquet, M., Carton, J.A., Cohn, S.E., Dance, S.L., Losa, S.N., Nichols, N.K., Potthast, R., Waller, J.A., Weston, P., 2018. On the representation error in data assimilation. Q. J. R. Meteorol. Soc. 144, 1257–1278. doi:doi:10.1002/qj.3130.

Karbou, F., Gérard, E., Rabier, F., 2006. Microwave land emissivity and skin temperature for AMSU-A and -B assimilation over land. QJRMS 132, 2333–2355.

Kazumori, M., English, S.J., 2015. Use of the ocean surface wind direction signal in microwave radiance assimilation. QJRMS 141, 1354–1375. URL: https://rmets.onlinelibrary.wiley.com/doi/abs/10.1002/qj.2445, doi:doi:10.1002/qj.2445.

Lean, K., Bormann, N., 2025. Evaluation of hyperspectral MW for NWP: Simulation framework consolidation. ESA Contract 4000145264/24/NL/IB/ab doi:10.21957/2752effd7a.

Lean, K., Bormann, N., Ackermann, J., Di Michele, S., Accadia, C., Hewison, T., 2026a. Ensemble-based evaluation of the forecast impact expected from EPS-Sterna. part II: Adding the 325 GHz channels. Monthly Weather Review 154, 487–503. doi:10.1175/MWR-D-25-0119.1.

Lean, K., Bormann, N., Healy, S., 2021. Technical Note 2 for ESA Contract No. ESA 4000130590/20/NL/IA: WP-2000 Calibration of EDA spread and adaptation of the observation error model. ESA Contract 4000130590/20/NL/IA Technical Note 2 URL: https://www.ecmwf.int/node/20302, doi:10.21957/1auh0nztg.

Lean, K., Bormann, N., Healy, S., Ackermann, J., Di Michele, S., Accadia, C., 2026b. Ensemble-based evaluation of the forecast impact expected from EPS-Sterna. part I: Evaluation of 50 and 183 ghz channels. Monthly Weather Review 154, 469–485. doi:10.1175/MWR-D-25-0118.1.

Lean, K., Bormann, N., Healy, S., English, S., Schuettemeyer, D., Drusch, M., 2025. Assessing forecast benefits of future constellations of microwave sounders on small satellites using an ensemble of data assimilations. Quarterly Journal of the Royal Meteorological Society e4939. doi:10.1002/qj.4939.

Lui, G., 2008. A database of microwave single-scattering properties for nonspherical ice particles. Bull. Am. Met. Soc. , 1563–1570.

Ma, Z., Bormann, N., Lean, K., Duncan, D., Berbery, E., Kalluri, S., 2025. Forecast impact assessment of SMBA using the EDA method. ECMWF Technical Memorandum No.929, 26pp. doi:10.21957/f952cd9118.

Maddy, E.S., Iturbide-Sanchez, F., Boukabara, S.A., 2024. Toward the next generation of microwave sounders: Benefits of a low-earth orbit hyperspectral microwave instrument in all-weather conditions using ai. IEEE Journal of Selected Topics in Applied Earth Observations and Remote Sensing 17, 4235–4246. doi:10.1109/JSTARS.2024.3356858.

Okamoto, K., McNally, A.P., Bell, W., 2014. Progress towards the assimilation of all-sky infrared radiances: an evaluation of cloud effects. Q. J. R. Meteorol. Soc. 140, 1603–1614.

Racette, P., Lang, R.H., 2005. Radiometer design analysis based upon measurement uncertainty. Radio Science 40. doi:https://doi.org/10.1029/2004RS003132.

Saunders, R., Hocking, J., Turner, E., Havemann, S., Geer, A., Lupu, C., Vidot, J., Chambon, P., Köpken-Watts, C., Scheck, L., Stiller, O., Stumpf, C., Borbas, E., 2020. RTTOV-13 science and validation report. EUMETSAT NWP SAF, version 1.0 URL: https://nwp-saf.eumetsat.int/site/software/rttov/documentation/.

Saunders, R., Hocking, J., Turner, E., Rayer, P., Rundle, D., Brunel, P., Vidot, J., Roquet, P., Matricardi, M., Geer, A., Bormann, N., Lupu, C., 2018. An update on the RTTOV fast radiative transfer model (currently at version 12). Geosci. Model Dev. 11, 2717–2737. doi:https://doi.org/10.5194/gmd-11-2717-2018.

Steele, L., Bormann, N., Geer, A., Chrust, M., Duncan, D., 2025. Enhancing the exploitation of all-sky microwave sensors at ECMWF using inter-channel error correlations. Eumetsat/ECMWF Fellowship Programme Research Report RR68. doi:10.21957/53801337ec.

Tan, D.G.H., Andersson, E., Fisher, M., Isaksen, L., 2007. Observing-system impact assessment using a data assimilation ensemble technique: Application to the ADM-Aeolus wind profiling mission. Quart. J. Roy. Meteor. Soc. 133, 381–390.

Weston, P., Bell, W., Eyre, J.R., 2014. Accounting for correlated error in the assimilation of high-resolution sounder data. Quarterly Journal of the Royal Meteorological Society 140, 2420–2429. doi:https://doi.org/10.1002/qj.2306.

Weston, P., Bormann, N., 2018. Enhancements to the assimilation of ATMS at ECMWF: Observation error update and addition of NOAA-20. EUMETSAT/ECMWF Fellowship Programme Research Report , 28 ppURL: https://www.ecmwf.int/node/18744.